Development and verification of the fluid model for organic degradable maize straw seedling raising bowl

Jingbo Qu[1,2], Xiaopei Qi[1,2], Fuxin Wang[1,2], Yuchen Che[1,2], Shaolong Che[1,2], Yuqi Zhang[1,2], Yong Sun[1,2*]

(1. *College of Engineering, Northeast Agricultural University, Harbin 150030, China*;
2. *Key Laboratory of Pig-breeding Facilities Engineering, Ministry of Agriculture, Harbin 150030, China*)

Abstract: The annual yield of maize straws is almost exclusively treated by field burning in China. Therefore, exploring the potential utilization value of maize straws is important to further realize modern agriculture in China. Maize straw-based organic degradable seedling bowls, formulated with pig manure and biogas slurry as binding agents, can be utilized for planting seedlings. These seedling bowls serve to supply organic material to the seedlings, thereby aiding in pest prevention and enhancing soil fertility. The vacuum filter suction forming method was proposed to prepare degradable seedling bowls according to its characteristics. Using the theory of fluid flow, drag reduction, and pressure drop control, the fluid model of seedling bowl material in the process of vacuum filtration was established, and the preparation of seedling bowl mold resistance factors was analyzed. The verification test showed that the pressure change interval and the blowing pressure are important factors influencing the formation of the wet body of the seedling bowl. This study provides theoretical support and guidance for the preparation of biodegradable seedling pots.

Keywords: degradable seedling bowl, maize straws, resistance factors, fluid model, vacuum suction filter method
DOI: 10.25165/j.ijabe.20251801.5879

Citation: Qu J B, Qi X P, Wang F X, Che Y C, Che S L, Zhang Y Q, et al. Development and verification of the fluid model for organic degradable maize straw seedling raising bowl. Int J Agric & Biol Eng, 2025; 18(1): 43–50.

1 Introduction

China boasts a substantial annual maize straw yield, reaching about 300 million tons per year[1-3]. However, due to the small-scale, dispersed, and independent nature of agricultural structures in China, maize straws are primarily disposed of through field burning, alongside their use as livestock feed[4,5]. Therefore, broadening the industrial chain by finding the potential utilization value of maize stalks and realizing the sustainable development of agriculture is a crucial approach for China to further realize modern agriculture[6,7]. Biologically generated hydrogen and methane derived from renewable sources such as biomass, wastewater, and organic wastes are collectively termed as "biohydrogen"[8,9]. Waste and/or wastewater containing organic pollutants serve as carbon and energy sources for the microbes used for biohydrogen production[10]. Biohydrogen can be synthesized through two primary approaches: photosynthetic (photo-autotrophic and photo-heterotrophic) and fermentative pathways[11,12]. Biohydrogen production involves direct photolysis, indirect photolysis, photo-fermentation, or dark fermentation[13,14]. Each biohydrogen production method presents distinct advantages and drawbacks. Collectively, biological strategies for hydrogen production hold significant potential for large-scale H_2 generation, as microorganisms have the ability to produce hydrogen from abundant and renewable feedstock. This renders the biological process a competitive alternative to traditional chemical methods like reforming and gasification for hydrogen production[15]. Agricultural residues, as well as food wastes and effluents from industrial processes such as sugar refining, olive processing, and cheese production serve as appropriate feedstocks for biohydrogen generation processes.

Although traditional plastic seedling raising bowls are cost-effective, their non-degradable nature poses significant environmental challenges. Moreover, the lack of biodegradability in plastic containers hinders healthy seedling root growth, potentially leading to root rot and damage, consequently impacting crop survival rates[16]. In dark-fermentation, bacteria thrive on organic substrates, breaking them down through oxidation to enhance biomass production and metabolic energy. In anaerobic conditions, to uphold cellular electrical neutrality, the electrons produced during substrate oxidation are balanced by reducing protons to H_2. Dark-fermentation processes typically exhibit a rapid H_2 production rate and are unaffected by light exposure. When utilizing various organic wastes as carbon sources, dark fermentative H_2 production predominantly results in the generation of acetic and butyric acid, along with other volatile fatty acids (VFAs), ultimately contributing to soil enrichment[17,18]. Fortunately, organic degradable seedling bowls, composed of maize straws as raw material and pig manure and biogas slurry as adhesive, can solve the above problems. Firstly, all constituent raw materials are organic and can be planted alongside seedlings to furnish organic matter and improve soil fertility. Secondly, due to the loose and porous structure of raw materials, plant roots can fully absorb water and other nutrients[19]. Finally, the utilization of pig biogas slurry as an adhesive in the raw materials provides a rich source of essential elements required for plant growth. This not only aids in pest prevention and control but

Received date: 2023-10-14 **Accepted date:** 2024-10-09
Biographies: Jingbo Qu, MS, Associate Professor, research interest: anaerobic fermentation, Email: ququjingbo@126.com; **Xiaopei Qi**, MS, research interest: anaerobic fermentation, Email: 3116064162@qq.com; **Fuxin Wang**, MS, research interest: anaerobic fermentation, Email: 1094139465@qq.com; **Yuchen Che**, MS, research interest: anaerobic fermentation, Email: cheyuchen0828@163.com; **Shaolong Che**, MS, research interest: anaerobic fermentation, Email: 703613465@qq.com; **Yuqi Zhang**, MS, research interest: anaerobic fermentation, Email: 15035451306@163.com.
***Corresponding author: Yong Sun**, Professor,research interest: anaerobic fermentation. College of Engineering, Northeast Agricultural University, Harbin 150030, China. Tel: +86-13836145034, E-mail: sunyong@neau.edu.cn.

also improves soil fertility[20-23]. The preparation of slurry for seedling bowls necessitates a specific apparent viscosity. The complex bridging interactions among fiber molecules in the raw materials require enhancements in the efficiency of seedling bowl preparation using traditional processes[24,25]. The degradable seedling bowl yield achieved through constant pressure adsorption is about 80%, with the total process duration averaging about 70 s. However, the fiber distribution in the resultant seedling bowl is uneven, highlighting the need to strengthen its mechanical integrity[26].

The fluid model of the raw material serves as a fundamental component in the vacuum filtration forming method for preparing degradable seedling bowls. This study aimed to utilize data derived from the analysis of raw material flow characteristics during the preparation process of seedling raising bowls to establish a pertinent fluid model. Numerical simulations were conducted to analyze the factors influencing mold resistance and propose necessary modifications. Finally, several key indices affecting the seedling bowl system in the preparation process were identified.

2 Materials and methods

2.1 Properties of porous media

The main medium components in the seedling bowl consist of multiple phases, including liquid phase, gas phase, and solid phase[27]. Due to the existence of solid phase, the whole seedling bowl forms a porous structure, with the gas phase and liquid phases occupying these voids. Some parameters require definition before establishing the model.

2.1.1 Porosity

The porosity index reflects the pore structure characteristics of the material, it can be expressed as:

$$e = \lim \frac{\Delta V_r}{\Delta V} \tag{1}$$

where, e represents void ratio; ΔV is the volume of skeleton in porous media, with dimension in L^3.

2.1.2 Specific surface area

The specific surface area of the porous media is the total surface area of all particles within the porous media volume:

$$a = \frac{\Delta A_t}{\Delta V} \tag{2}$$

where, a is specific surface area, L^{-1}; ΔA_t denotes the total surface area of all particles in volume ΔV, with dimension in L^3.

2.1.3 Curvature

The curvature degree is a measure of the bending degree of the capillary channel and is defined as the square of the ratio of the sample length to the total length of liquid motion.

$$\tau = \left(\frac{L}{L_e}\right)^2 \tag{3}$$

where, τ represents the curvature of porous media; L_e is the length of the fluid variable, mm; L denotes the sample length, mm. Obviously, $0<\tau<1$, the higher the bending degree, the smaller the value of τ.

2.2 Properties of fluids

2.2.1 Density of fluids

Density refers to the quantity of material present in a unit volume:

$$\rho = \frac{M}{V} \tag{4}$$

where, ρ is the density of the liquid, kg/m³; M represents the mass of the substance contained in the fluid of volume V, kg.

2.2.2 Unit weight

The relationship between the gravity and the density of the fluid:

$$\gamma = \rho g \tag{5}$$

where, γ signifies the unit weight, kg; g denotes the acceleration of gravity, which is 9.8 m/s².

2.2.3 Viscosity of fluids

Derived from Newton's law of internal friction:

$$\tau = \mu \frac{du}{dy} \tag{6}$$

where, τ denotes shear stress, Pa; $\frac{du}{dy}$ represents the shear deformation rate of the fluid, s^{-1}; μ denotes the dynamic viscosity of the fluid, Pa·s.

2.3 Establishment of fluid model in vacuum filtration molding

2.3.1 The mixture flow of straw, pig manure, and biogas slurry

In the presence of an air pressure differential generated by the pneumatic device, the raw material undergoes filtration to separate the filtrate through the filter net and mold. Assuming a filter with a complex cross-sectional shape characterized by porosity ε(%) and its specific surface area a, the whole flow distance is set to long pipe of length L. The pipe diameter is calculated from the porosity and the specific surface area of the straw fiber[28]. The formula for the flow rate of the filtrate during the molding process is obtained as follows:

$$u = \frac{1}{Z}\frac{\varepsilon^3}{a^2(1-\varepsilon)^2}\left(\frac{\Delta P_c}{\mu L}\right) \tag{7}$$

where, Z represents the proportional constant, which is related to the fiber quality of the straw in the raw material and can be measured experimentally. In fact, the speed of the filtrate during the suction filtration process is not constant, and the resistance increases as the thickness of the molding increases, resulting in a gradual decrease in its velocity.

The speed at any moment is as follows:

$$u = \frac{dv}{Adt} = \frac{1}{Z}\frac{\varepsilon^3}{a^2(1-\varepsilon)^2}\left(\frac{\Delta P_c}{\mu L}\right) \tag{8}$$

The formula above illustrates that the key factors affecting the molding speed during the molding process are mainly the pressure difference on both sides of the model, the thickness of the filter screen, the dynamic viscosity of the raw material, and the physicochemical characteristics of the straw fiber. The resistance formula of the filtrate can be further deduced from the above process.

2.3.2 Resistance of mixture of straw and pig manure biogas during filtration molding

In the above formula, given that the raw material ratio remains constant, it can be considered that ε is a constant, and the fiber shape and size of maize stalk are substantially the same, so a is a constant.

If $\frac{\varepsilon^3}{Za^2(1-\varepsilon)^2} = M$, as the coefficient of permeation layer, it can reflect the characteristics of the fiber in maize stalk. Generally, the value of Z is 5. If $y = \frac{1}{M}$, we have the following equations:

$$y = \frac{1}{M} = \frac{5a^2(1-\varepsilon)^2}{\varepsilon^3} \tag{9}$$

The aforementioned formula indicates that a smaller value of ε corresponds to a finer and denser final product, resulting in increased resistance to the flow of raw materials.

2.3.3 Establishment of filtration equation

Assuming that the net volume of seedling bowl is n m^3 of 1 m^3 raw material, the relationship between thickness and V can be expressed as follows:

$$L = \frac{nV}{A} \tag{10}$$

In practical applications, consideration should be given to the thickness of the filter screen and the mold. The correction formula for the filtrate velocity under these circumstances is as follows:

$$\frac{dV}{Adt} = \frac{\Delta P_w}{\mu R_w} \tag{11}$$

where, ΔP_w represents the pressure difference provided by the pneumatic device, Pa; while μR_w is the medium resistance, Pa. Given that the nursery area is equivalent to the filter screen area, the filtration velocity is calculated as follows:

$$\frac{dV}{Adt} = \frac{\Delta p_m + \Delta p_c}{\mu(R_w + R)} = \frac{\Delta p}{\mu(R_w + R)} \tag{12}$$

where, $\Delta p_m + \Delta p_c$ represents the total pressure drop on both sides of the filter, Pa. If the thickness of the seedling bowl is L_e, m; then:

$$\gamma L_e = R_m \tag{13}$$

Thereupon:

$$\frac{dV}{Adt} = \frac{\Delta p}{\mu(R_w + R)} = \frac{\Delta p}{\mu\left(\gamma L_e + RL\right)} \tag{14}$$

If the liquid volume of the raw material needed to form a seedling bowl with thickness of L_e is V_e, then

$$L_e = \frac{nV_e}{A} \tag{15}$$

where, V_e is the equivalent filtrate volume of the filter medium, L^3.

Thereupon:

$$\frac{dv}{dt} = \frac{A^2 \Delta p}{\mu\gamma n(V + V_e)} \tag{16}$$

Therefore, the relationship between resistance, pressure, and velocity is obtained.

3 Results and discussion

The relationship between pressure, resistance, and velocity reveals that the resistance encountered during the adsorption molding of the seedling bowl emanates from abrupt changes in the suction hole section, the length of the suction hole, and the quality of hole processing. To comprehensively elucidate the impact of various influencing factors on mold formation, it is imperative to develop a model that delineates the interaction between the mold and the seedling bowl.

3.1 Problem description of the parameters of forming die

To mitigate mold resistance losses, strategies such as reducing the length of the suction hole, minimizing structural alterations in the suction section, and substituting high-quality suction holes with alternative methods can be implemented[29]. In the finite element analysis conducted in this study, enhancements were made to the varying angles of the suction hole and conical hole to alleviate the abrupt changes in the weakening suction hole section. The impact of suction hole quality on pressure loss was examined by altering the surface roughness of the suction hole, while the effect of hole length on pressure loss was investigated by modifying between long and short holes.

The roughness of the subject during processing is 6.3. The ideal smooth model, chamfer model, and tapered hole model have a hole length of 0.02 m. Its aspect ratio is 10, which is greater than 4. Conversely, the short hole model has a suction hole length of 0.005 m, accompanied by an aspect ratio of 2.5, which is less than 4.

The geometric dimensions are as follows: the pressure flow hole measures 0.020 m in length and 0.022 m in height; the radius hole of ideal model and rough model is 0.004 m. In the ideal model, a chamfer of 0.0004 m is incorporated post-machining, while all other dimensions remain consistent with the rough model. The conical pore model features a pressure outflow hole diameter of 0.003 m and a pressure inlet hole diameter of 0.0065 m.

The analysis region models for each model are illustrated as follows (Figures 1-4):

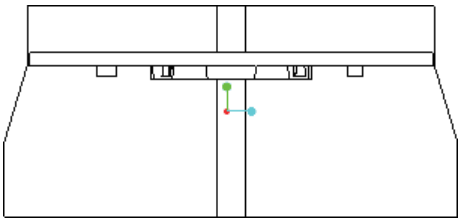

Figure 1 Smooth and added roughness model (main view)

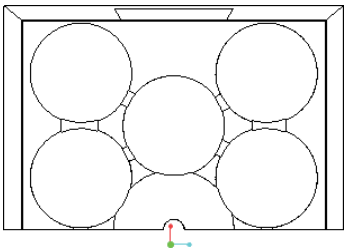

Figure 2 Smooth and added roughness model (top view)

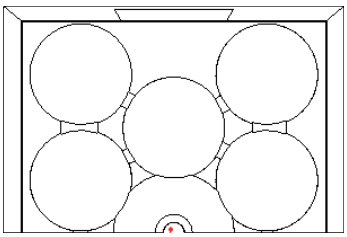

Figure 3 Chamfer model

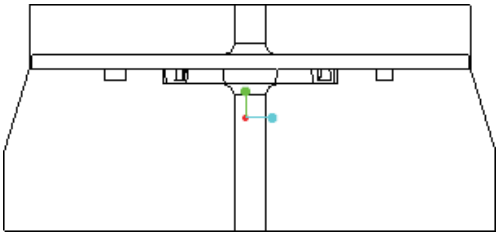

Figure 4 Conical hole model

In this study, FLOTRAN (Ansys, America) was used to make corresponding modeling and analysis. The computer simulation model constructed encompasses numerous suction holes in the convex die. The mesh division of the suction filter convex die and structures such as the material box are shown in Figure 5. The pressure-based solver was selected for solution. Given the transient nature of the observed state, the time setting is configured to an unsteady state, with results presented in the form of apparent velocity. The viscous model is initiated to account for fluid viscosity effects. The operational sequence entails: Pressure Based -

Unsteady - Superficial Velocity - Viscous Model. In the component model, the component transport model is chosen, while the mixture material adopts the mixed mode. The specific operational sequence comprises: Species Model - Species Transport - Mixture Material - Mixture Template. In the material control panel, the material type is defined as a mixed fluid with the specific steps of Materials - Mixture. The liquid flow exhibited laminar characteristics, with a pressure difference of 5 N between the inlet and outlet. All wall surfaces were assigned no-slip boundary conditions. The fluid behavior was assumed to be incompressible, with the average density of the mixture set at 1.005×10^3 kg/m^3, with a viscosity of 0.002 Pa·s.

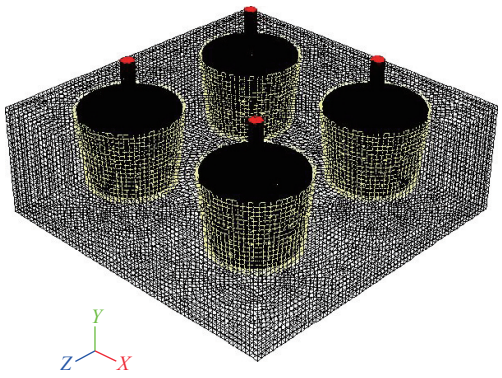

Figure 5 Meshing of the suction filter forming mold model

Initially, maize straws were utilized as raw material to fabricate the seedling bowl. The apparent viscosity, cellulose composition, and rheological properties of the raw materials were determined. Subsequently, the impact of slurry suction time on the formation of the green body of the seedling bowl was investigated[30]. To assess the accuracy and effectiveness of the model, the simulation results were compared with the previous test results, as outlined in Table 1. Analysis of the table reveals a minimal error between the experimental results and simulated values, falling within a narrow margin of 2.2%. This alignment signifies that the four models closely adhere to the experimental conditions. Therefore, the subsequent results are based on these four models.

Table 1 Numerical simulation and experimental results under different models

Model	Flow/ m^3·h^{-1}	Pressure/Pa		
		Simulation value	Experimental result	Relative error
Ordinary smooth mold	5.0	10.64	10.75	1.03%
	7.5	20.02	20.39	1.85%
	10.0	32.78	33.22	1.34%
Common rough mold	5.0	11.27	11.48	1.86%
	7.5	21.65	22.12	2.17%
	10.0	36.78	37.04	0.71%
Chamfer smooth mold	5.0	12.78	12.99	1.64%
	7.5	22.68	22.85	0.75%
	10.0	37.64	37.88	0.64%
Conical hole mold	5.0	13.06	13.25	1.45%
	7.5	23.76	24.01	1.05%
	10.0	39.02	39.24	0.56%

3.2 Analysis of factors affecting resistance of seedling bowl during adsorption molding

When the viscous fluid flows along a fixed boundary, the fluid can exhibit an arbitrary motion state. Since the flow velocity is zero at the mixture boundary, the upward velocity gradient of the boundary surface method is non-zero, leading to the presence of shear force on the boundary surface[31,32]. The action of shear forces on the mixture results in the dissipation of energy outwardly in the form of heat energy, necessitating additional energy input to uphold operational efficiency and the shaping quality of the seedling bowl.

In accordance with resistance theory, the size of vortices is dictated by the Reynolds number, whereas the vortex size is influenced by the relative roughness[33]. The escalation in the rate of drag reduction for smoother surfaces is attributed to the augmentation of local vortex size induced by the boundary of the mixed liquid, which enlarges with an increase in the relative roughness rate while maintaining a constant Reynolds number. The variation in the drag reduction rate for smoother surfaces ranges notably between 0.045 and 4.300 under different relative roughness. The influence of smoothness on the resistance coefficient in the inner flow of the mixture is obvious. Drag reduction prioritizes smooth drag reduction followed by viscous drag reduction. It is imperative to enhance the surface quality of both the back cavity and suction surface of the mold, thereby minimizing resistance in the adsorption molding process and enhancing production efficiency. To ensure surface roughness accuracy remains below 7.5, the diameter of the drill hole must not exceed 15 mm in this study.

3.3 Analysis of finite volume results

The provided images depict the output results following finite element analysis. The velocity and pressure change graphs illustrate speed and pressure values, respectively, measured in international units. The horizontal coordinates represent the relative positions of the points along the suction aperture near the inlet of the suction holes in each model.

3.3.1 Analysis results of ideal smooth suction hole model

The axial pressure change trend chart of the suction hole reveals that the primary pressure loss region occurs in the suction section, where the loss value significantly exceeds that of the surrounding areas of the suction hole (Figure 6). Therefore, modifying the design of the mold suction hole exerts a considerable impact on the pressure resistance of the mold, aligning with the theoretical model as discussed earlier. Additionally, examination of the velocity contour map indicates the formation of a vortex at the suction hole outlet, contributing to localized pressure losses.

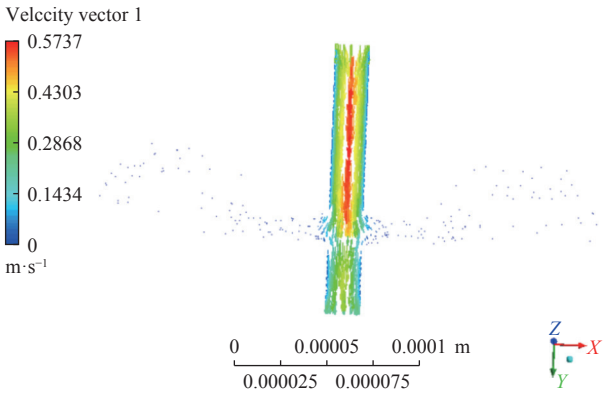

Figure 6 Exit velocity diagram

3.3.2 Analysis results of adding roughness model

Figure 7 shows the velocity diagram of the holes in the model after adding roughness. From this figure, the vertical coordinates indicate the velocity of the holes in the roughness model. A comparison with the model under ideal conditions reveals a notable

decrease in the speed of each point, accompanied by a corresponding reduction in speed differentials. As the roughness value increases, the inherent resistance of the mold to the mixed liquid intensifies, leading to elevated fluid pressures within. Hence, it is imperative to enhance processing accuracy to improve the surface quality.

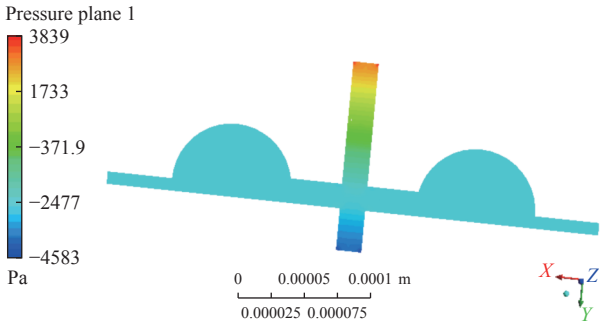

Figure 7 Vertical profile pressure nephogram

3.3.3 Results of chamfer model analysis

The pressure difference of the chamfer model was 28%-35% lower than that of the mold without casting chamfering. This practice ensures template uniformity, enhances fluid velocity, accelerates filtrate precipitation, reduces internal mixture losses, and notably diminishes vortex intensity and range at the hole's inlet and outlet (Figure 8).

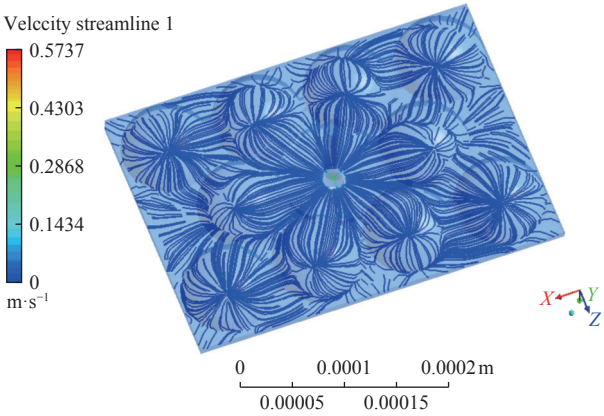

Figure 8 Cross-sectional flow pattern

3.3.4 Analysis result of tapered hole model

Compared with the inlet and outlet of equal diameter, the pressure of the conical hole model was gradually increased at the hole entrance. This effect mitigated the hindrance of the mold on the mixture, augmented fluid kinetic energy, and potentially increased speed between the two holes by approximately 50%. However, the results showed that the method could reduce the uniformity of the seedling growing bowl, rendering it an inadvisable strategy (Figure 9).

Finally, by shortening the length of the suction hole, minimizing abrupt changes in the suction hole section, and enhancing the processing quality of the suction hole, it is feasible to mitigate the pressure loss attributable to the mold itself and alleviate the inherent resistance posed by the mold.

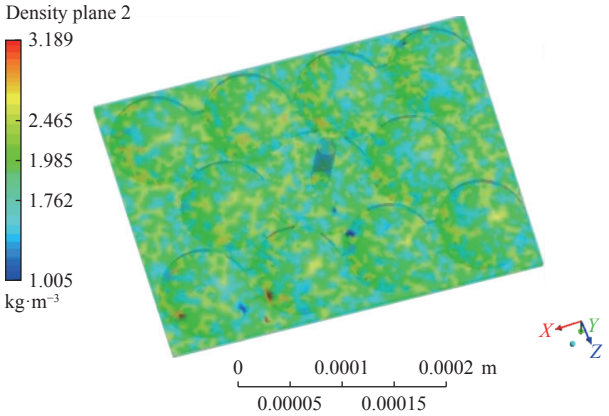

Figure 9 Lumen density map

3.4 Analysis results of constant pressure adsorption

In the simulation of pot-making by constant pressure adsorption, the velocity nephograms at 5 s, 10 s, 15 s, and 20 s were selected, as shown in Figure 10.

During the constant pressure adsorption process, the designated negative pressure value must meet the requisite pressure to enhance the resistance of the wet billet in the subsequent stages. Thus, in the initial stage of adsorption forming, there is a higher material-liquid flow rate within the bin. As the wet billet attains a certain thickness, the resistance of the wet billet significantly escalates, thereby impeding material-liquid flow within the bin and affecting the wet billet in the seedling raising bowl. Consequently, the precipitation rate decreases. The precipitation rate of seedling raising bowl decreases compared with the initial rate at 10 s and remains stable during 10-15 s. This indicates that during the first 10 s of adsorption, larger fibers are first lapped and formed, leading to a continuous increase in the thickness of the porous medium of the wet billet. During this period, the resistance of the wet billet increases gradually due to the filling of smaller fibers, resulting in a weakened force of the material liquid and a subsequent decrease in flow rate. In the previous experiment of preparing the seedling bowl with constant pressure, the precipitation rate of the wet billet was faster in the early stage of adsorption, yet the rate of increase in the wet billet thickness diminished swiftly. However, during this period, the thickness of the wet billet did not reach the required thickness. Subsequently, at a lower speed, the wet billet thickness exhibited gradual augmentation and required approximately 40 s to attain the specified thickness, with the outer layer retaining moisture. Following the drying of the wet billet, distinct characteristics are observed: the initial wet billet layer appears rough, the middle layer is fine, and the outer layer exhibits larger voids. This observation suggests that the adsorption force of fibers fluctuates during the wet billet formation process, indicating a staged decrease in material-liquid velocity, which is consistent with the simulation results.

3.5 Verification experiments

3.5.1 Trial production of degradable seedling bowl

To validate the conclusions drawn in the preceding section, a small-scale production of seedling raising bowls was conducted following the outlined manufacturing process, and the key characteristics were analyzed. Four sets of molds for the seedling raising bowl were fabricated, including an ordinary smooth mold, an ordinary rough mold, a chamfer smooth mold, and a conical hole mold. All other factors remained constant except for the specified parameter variations in the four molds. Each group of molds was used to produce 100 groups of seedling bowls, with a pressure

sensor integrated to measure the mold pressure throughout the bowl-making process. The influence of smoothness degree, chamfering, and conical hole on the pressure of mold in the process of production were systematically analyzed.

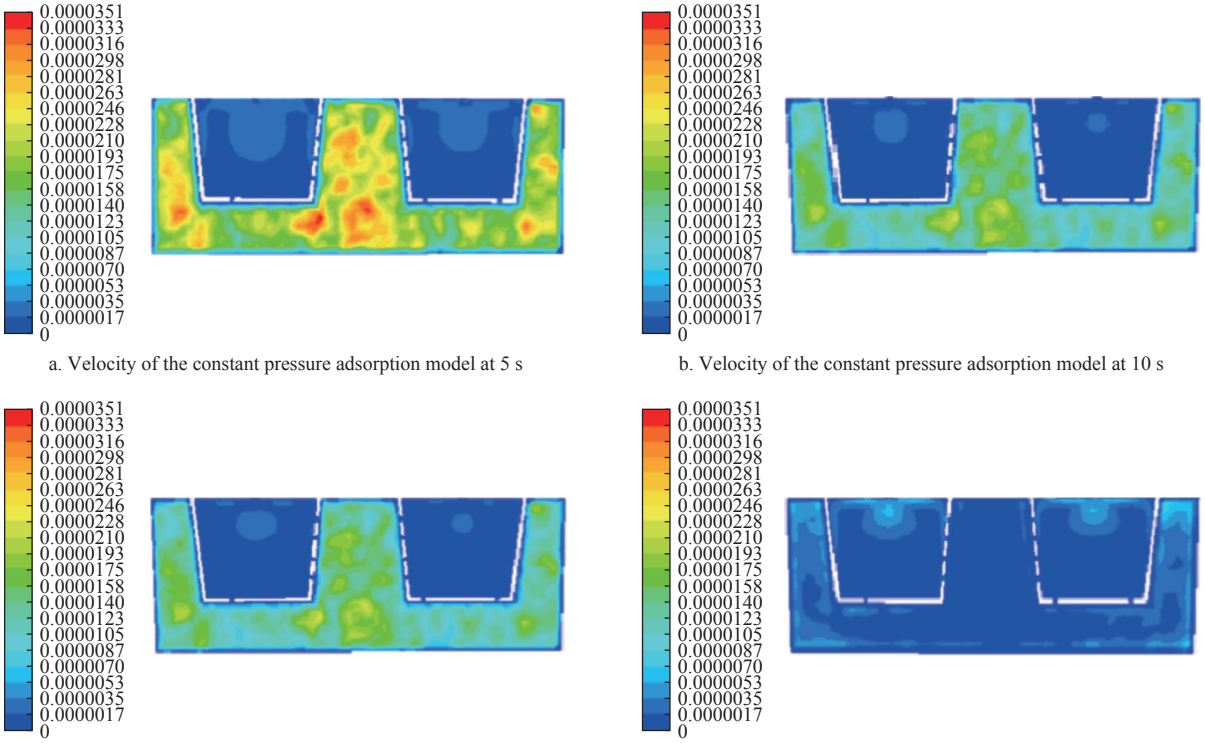

a. Velocity of the constant pressure adsorption model at 5 s

b. Velocity of the constant pressure adsorption model at 10 s

c. Velocity of the constant pressure adsorption model at 15 s

d. Velocity of the constant pressure adsorption model at 20 s

Figure 10 The velocity nephogram during constant pressure adsorption

3.5.2 Test indicators

In the process of preparing the seedling bowl, the manufacturing parameters of the mold can play a key role in the extrusion resistance and water retention ability, thereby exerting a decisive role in the seedling growth. Therefore, the test factors are the smoothness, chamfer, and conical hole of the mold.

1) Smoothness: the smooth mold and the ordinary rough mold were used to produce seedlings, respectively, and the pressure inside the internal mold pressures were compared during production.

2) Chamfer: the ordinary smooth mold and the smooth chamfering mold were used to produce seedling bowls, respectively, and the internal mold pressures were compared between the two during production.

3) Conical hole: the common smooth mold and the conical hole mold were used to produce seedling bowls, and the internal mold pressures were compared.

3.5.3 Test equipment

All tests were carried out on the basis of pneumatic test bench, comprising experimental benches, working pump stations, pneumatic components, electrical control units, sensor units, and so on. The specific dimensions of the test bench are as follows: length×width×height=1700 mm×590 mm×1900 mm, with an approximate weight of 170 kg. The pump (Agilent Technologies Inc., China) operates on an input voltage of AC 220 V/50 Hz, features a motor power of 125 W, a rated output pressure of 0.8 MPa, and an air pump volume of 10 L. The programmable logic controller (PLC) utilized the Japan Omron series (Omron, Japan), featuring 20 I/O ports with relay output configuration. The supply voltage is AC 220 V/50 Hz, while the control voltage is DC 24 V, offering manual, automatic, sequential, and additional control functionalities. The molds for seedling preparation were integrated into the pneumatic system configuration. The raw materials comprised a mixture of maize stalks and pig manure slurry, specifically tailored for the cold regions of northeastern areas, and were thoroughly stirred.

3.5.4 Test results and analysis

The pressure was adjusted to 1-4 T, and the number of revolutions of the hydraulic mold driven by the motor was 500-2000 r/min. Subsequently, the crop stalk mixed with adhesive was placed in the mold to make the mash. The test results are shown in Table 2. The single molding rate of a smooth ordinary mold reached 80.2%, while that of the ordinary molds was only 75.4%. The single molding rates of chamfering molds and tapered hole molds were 84% and 92%, respectively.

Table 2 Four mold forming results

Model	Primary molding rate/%	Relative mean pressure/Pa	Pressure breakage rate/%		
			20 kg	40 kg	60 kg
Ordinary smooth mold	80.2	80-85	3.92	6.14	15.90
Common rough mold	75.4	100	4.55	7.20	47.20
Chamfer smooth mold	84.0	65-82	3.56	5.92	17.50
Conical hole mold	92.0	50	2.33	4.32	10.10

Upon reaching a bearing capacity of 20 kg, the breakage rate of all four seedling raising bowls was less than 5.0%. However, as the load was raised to 60 kg, the breakage rate of ordinary smooth mold, smooth chamfering mold, conical hole mold, and ordinary rough mold were 15.9%, 17.5%, 17.5%, and 17.5%, respectively. There were significant differences among different molds. Li has developed a new type of rice seedling carrier termed the rice straw seedling tray[34]. The study substituted the modified starch-based adhesive with a thermosetting adhesive binder, thereby reducing

preparation constraints such as forming pressure, forming temperature, and dwell time. Utilizing anaerobic fermentation biogas slurry derived from pig manure and maize straw as raw materials for seedling bowl production, the process demonstrated enhanced simplicity and operational ease. These findings offer valuable insights for future research endeavors and potential industrial applications in the realm of seedling raising bowls. Related research found that a seedling tray made of straw and manure was completely degraded over 40 days, with an observed enhancement in the degradation rate of straw[35,36]. Additionally, the seedling bowl prepared by this study exhibited favorable degradation characteristics. Future investigations will focus on evaluating alterations in parameters such as water immersion capacity, permeability, and air permeability.

4 Conclusions

By implementing a rational design for the hydraulic mold of the straw seedling bowl-making machine, this study successfully addressed issues prevalent in existing synthetic straw seedling bowl production, including excessive mold hydraulic pressure, subpar forming outcomes, and susceptibility to formation failures. Concurrently, enhancements were made to the mold structure, thereby bolstering the strength of the straw seedling bowl, optimizing the mold's technological process, improving the single forming rate, and reducing production costs. The moisture content of the wet billet decreases with the increase of the adsorption pressure gradient and increases with the increase of the pressure change interval. Excessive or inadequate blowing pressure hinders the demolding process of the wet billet, with an optimal blowing pressure of 250 kPa facilitating a smoother blowing operation. These findings underscore the significance of pressure change interval timing and blowing pressure as critical factors influencing the wet billet formation in seedling bowl production.

Acknowledgements

This work was supported by the National Natural Science Foundation of China (Grant No. 52206234).

[References]

[1] Cong H B, Zhao L X, Mašek O, Yao Z L, Meng H B, Huo L L, et al. Evaluating the performance of honeycomb briquettes produced from semi-coke and corn stover char: Co-combustion, emission characteristics, and a value-chain model for rural China. Journal of Cleaner Production, 2020; 244: 118770.

[2] Xu Y H, Song Y N, Jiang H, Zhang H Q, Sun Y. Effect of vacuum negative pressure aerobic hydrolysis pretreatment on corn stover anaerobic fermentation. Int J Agric & Biol Eng, 2023; 16(2): 241–248.

[3] Xu D Z, Ma C L, Wu M J, Deng Y, He Y C. Improved production of adipic acid from a high loading of corn stover via an efficient and mild combination pretreatment. Bioresource Technology, 2023; 382(9): 129196.

[4] Tang Z, Liang Y Q, Zhang B, Wang M L, Zhang H, Li Y M. Effects of multi-sequence combination forces on creep characteristics of bales during wheat harvesting. Int J Agric & Biol Eng, 2021; 14(5): 88–99.

[5] Wang T Y, Wang Z H, Wu Q, Zhang J Z, Quan L S, Fan B H, et al. Coupling effects of water and nitrogen on photosynthetic characteristics, nitrogen uptake, and yield of sunflower under drip irrigation in an oasis. Int J Agric & Biol Eng, 2021; 14(5): 130–141.

[6] Song Z Y, Xiong X, Huang G L. Ultrasound-assisted extraction and characteristics of maize polysaccharides from different sites. Ultrasonics Sonochemistry, 2023; 95: 106416.

[7] Liu J, Li C L, Qu Y T, Jia Z B, Li J H. Comparative life cycle assessment of the linear and circular wine industry chains: a case study in Inner Mongolia, China. Environmental Science and Pollution Research, 2023; 30: 87645–87658.

[8] Yan W C, Qu J B, Qu Y P, Yue T, Zhang Q G, Yi W M, et al. Effect of biochar addition on mechanism of heavy metal migration and transformation in biogas residue aerobic compost. Fermentation, 2022; 8(10): 523.

[9] Qu Y P, Qu J B, Yan W C, Yue T, Zhang Q G, Yi W M, et al. Influence of biochar on physico-chemical, microbial community and maturity during biogas residue aerobic composting process. Fermentation, 2022; 8(11): 623.

[10] D'Silva T C, Khan S A, Kumar S, Kumar D, Isha A, Deb S, et al. Biohydrogen production through dark fermentation from waste biomass: Current status and future perspectives on biorefinery development. Fuel, 2023; 350: 128842.

[11] Liu C Y, Sun Y, Li N, Zhang B, Liu J M. Improved energy utilization efficiency via adding solar radiant heating mode for traditional bioreactor to dispose straw: Experimental and numerical evaluation. Waste Management, 2019; 89: 303–312.

[12] Dong B C, Song C J, Li H B, Lin A J, Wang J C, Li W. Life cycle assessment on the environmental impacts of different pig manure management techniques. Int J Agric & Biol Eng, 2022; 15(3): 78–84.

[13] Lu C Y, Wang G T, Zhang Q G, Yang X D, Yu J C, Liu T, et al. Comparison of biorefinery characteristics: Photo-fermentation biohydrogen, dark fermentation biohydrogen, biomethane, and bioethanol production. Applied Enengy, 2023; 347: 121463.

[14] Nadeem F, Zhang H, Tahir N, Zhang Z P, Singhania R R, Shahzaib M, et al. Advances in the catalyzed photo-fermentative biohydrogen production through photo nanocatalysts with the potential of selectivity, and customization. Bioresource Technology, 2023; 382: 129221.

[15] Sharma M, Salama E, Thakur N, Alghamdi H, Jeon B-H, Li X K. Advances in the biomass valorization in bioelectrochemical systems: A sustainable approach for microbial-aided electricity and hydrogen production. Chemical Engineering Journal, 2023; 465: 142546.

[16] Zhu Z F, Wu G H, Ye B L, Zhang Y C. Reverse design and tests of vegetable plug seedling pick-up mechanism of planetary gear train with non-circular gears. Int J Agric & Biol Eng, 2023; 16(2): 96–102.

[17] Chai X L, Cao F S, Zhang C L, Zhong K, Jiang L J. Investigating the use of Aspergillus niger fermentation broth as a washing treatment for arsenic and antimony co-contaminated soil. Environmental Science and Pollution Research, 2023; 30(34): 82866–82877.

[18] Chang T T, Zhang Y J, Xu H L, Shao X H, Xu Q C, Li F L, et al. Osmotic adjustment and up-regulation expression of stress-responsive genes in tomato induced by soil salinity resulted from nitrate fertilization. Int J Agric & Biol Eng, 2018; 11(3): 126–136.

[19] Xu Q C, Li S J, Zhang J, Zhu J T, Pan H B. Design and test of self-propelled citrus seedling pots filling and placing machine. Int J Agric & Biol Eng, 2023; 16(1): 104–110.

[20] Fernandes D J, Ferreira A F, Fernandes E C. Biogas and biomethane production potential via anaerobic digestion of manure: A case study of Portugal. Renewable and Sustainable Energy Reviews, 2023; 188: 113846.

[21] Sun H, Cui X, Stinner W, Zhang L P, Ju X X, Guo J B, et al. Ensiling excessively wilted maize stover with biogas slurry: Effects on storage performance and subsequent biogas potential. Bioresource Technology, 2020; 305: 123042.

[22] Hao J J, Jia S F, Sun H, Chen G P, Zhang J X, Zhao Y B, et al. Effects of cow manure ratios on methane production and microbial community evolution in anaerobic co-digestion with different crop wastes. Int J Agric & Biol Eng, 2022; 15(5): 219–228.

[23] Zawadzinska A, Salachna P, Nowak J S, Kowalczyk W, Piechocki R, Łopusiewicz Ł, et al. Compost based on pulp and paper mill sludge, fruit-vegetable waste, mushroom spent substrate and rye straw improves yield and nutritional value of tomato. Agronomy, 2022; 12(1): 13.

[24] Ji J T, Yang L H, Jin X, Ma H, Pang J, Huang R B, et al. Design of intelligent transplanting system for vegetable pot seedling based on PLC control. Journal of Intelligent and Fuzzy Systems, 2019; 37(4): 4847–4857.

[25] Chen L T, Ma X, Wang C, Li H W, Li Z H, Chen X S, et al. Design and test of soft-pot-tray automatic embedding system for light-economical pot seedling nursery machine. Int J Agric & Biol Eng, 2020; 13(1): 91–100.

[26] Benavent-Celma C, McLaggan D, van West P, Woodward S. Survival of phytophthora cryptogea and phytophthora cactorum in commercial potting substrates for eucalyptus globulus plants. Agriculture, 2023; 13(3): 581.

[27] Ji J T, Sun J W, Jin X, Li M Y, Du X W. Development of a PVDF sensor for potted seedling clamping force of vegetable transplanting. Int J Agric & Biol Eng, 2019; 12(5): 111–118.

[28] Timene A, Haman-Djalo. Design of a five-bar duckbill-type mechanism for sorghum transplanting. Journal of Agricultural Engineering, 2023; 54(2): 1473.

[29] Lin Z M, Li S F, Liu C P, Wang L B, Zhang Y H. Thermal and flow characteristics of a channel formed by aligned round tube bank fins stamped with curve delta-winglet vortex generators. Thermal Science and Engineering Progress, 2021; 26(5): 101113.

[30] Yin J J, Wang Z L, Zhou M L, Wu L N, Zhang Y. Optimized design and experiment of the three-arm transplanting mechanism for rice potted seedlings. Int J Agric & Biol Eng, 2021; 14(5): 56–62.

[31] Awasthi M K, Asthana R, Agrawal G S. Viscous correction for the viscous potential flow analysis of capillary instability with heat and mass transfer. Journal of Engineering Mathematics, 2013; 80(1): 75–89.

[32] Awasthi M K, Yadav D, Agrawal G S. Viscous potential flow analysis of electrohydrodynamic rayleigh-taylor instability. Journal of Applied Fluid Mechanics, 2014; 7(2): 209–216.

[33] Togizbayeva B B, Sazambayeva B T, Karazhanov A A, Kenesbek A B, Cocosila M. Simulation of operation of neural network with purpose of utilisation of hydraulic actuators in complicated technical conditions. Int J Agric & Biol Eng, 2020; 13(1): 11–19.

[34] Li L H, Wan C, Zhang X Y, Li G Y. Improvement and optimization of preparation process of seedling-growing bowl tray made of paddy straw. Int J Agric & Biol Eng, 2014; 7(4): 13–22.

[35] Qi L Q, Zhang B, Ma Y C, Zhang W. Forming and degradation mechanism of bowl seedling tray based on straw lignin conversion. Agronomy, 2023; 13(2): 453.

[36] Qu Y P, Lv X Y, Qin N, Zhang K J, Ding X J, Luo L N, et al. Mechanism of ball milling pretreatment to improve the anaerobic digestion performance and energy conversion efficiency of corn straw. Fuel, 2024; 366: 131409.